NASA Technical Memorandum 105189

Microfracture in High Temperature Metal Matrix Laminates

Subodh K. Mital
University of Toledo
Toledo, Ohio

Christos C. Chamis and Pascal K. Gotsis
Lewis Research Center
Cleveland, Ohio

Prepared for the
32nd Structures, Structural Dynamics, and Materials Conference
cosponsored by the AIAA, ASME, ASCE, AHS, and ASC
Baltimore, Maryland, April 8-10, 1991

NASA

Microfracture in High Temperature Metal Matrix Laminates

Subodh K. Mital*
University of Toledo
Toledo, Ohio 43606

and

Christos C. Chamis and Pascal K. Gotsis
National Aeronautics and Space Administration
Lewis Research Center
Cleveland, Ohio 44135

Abstract

Computational simulation procedures are described to evaluate the composite microfracture behavior, establish the hierarchy/sequence of fracture modes and the influence of compliant layers and partial debonding on composite properties and microfracture initiation. These procedures are based upon three-dimensional finite element analysis and composite micromechanics equations. Typical results for the effects of compliant layers and partial debonding, microfracture initiation and propagation and the thermomechanical cyclic loading on SiC/Ti15 composite system are presented and discussed. The results show that interfacial debonding follows fiber or matrix fracture, and the thermomechanical cyclic loading severely degrades the composite integrity.

Introduction

Fiber reinforced composites have distinct advantages over conventional materials, which make them desirable candidates for applications in aerospace propulsion structures. Some of these advantages are well known : for example, high stiffness and strength to specific weight ratios. Other advantages include tailorable properties, high fatigue resistance, high

---

*NASA Resident Research Associate at Lewis Research Center.

fracture toughness etc. Practically all of these advantages derive from the inherent anisotropic and heterogeneous structure of fiber composites. This inherent structure, which provides composites with their distinct advantages, also substantially increases the complexity required to formally describe their structural behavior.

High temperature metal matrix composites (HTMMC), in particular, are potential candidate materials for applications demanding high operational temperatures. Over the past several years at NASA Lewis Research Center, metal matrix composite behavior has been evaluated using computational simulation procedures based on simplified micromechanics equations and three-dimensional finite element analysis. Among other things, the finite element method has been combined with mechanics of materials approach to evaluate the effects of partial debonding and fiber fracture on the global behavior of HTMMC. Also, similar analyses have been used to find ways to reduce high thermal residual microstresses by introducing a third phase or a compliant layer (CL) between the fiber and the matrix.

Recent research has been directed to quantify the effects of microfracture (fiber/matrix fracture, fiber-matrix interface debonding and interply delamination) on the global behavior of high temperature metal matrix laminates subjected to thermo-mechanical loading. This report outlines a procedure to evaluate composite microfracture behavior, establish the hierarchy and sequence of fracture modes. A 0.35 fiber volume ratio SiC/Ti15 unidirectional metal matrix composite and a 0.3 fiber volume ratio crossply (0/90/0) SiC/Ti15 laminate are evaluated for microfracture under various types of mechanical and thermal loads. The results obtained therefrom are presented and discussed. Defect and crack are used interchangeably in this report. For completeness, a brief summary of the previous relevant research is included prior to describing the recent research activities.

Compliant Layers Effects

Metal matrix composites have high residual stresses that develop during the fabrication process. These residual stresses result from (a) a large

temperature differential between the consolidation and the use temperatures and (b) the mismatch of coefficients of thermal expansions (CTE) of the fiber and the matrix. The presence of high thermal residual stresses can cause matrix microcracks which, in general, have adverse effects on mechanical properties and the thermomechanical fatigue endurance of the composites. Several possible ways have been suggested to reduce these residual microstresses, e.g. optimizing the processing history to minimize the thermal residual microstresses (ref. 1). One other possible method to reduce these high thermal residual microstresses is to introduce a third constituent, a compliant layer (CL), as a buffer between the fiber and the matrix. The objective of this compliant layer is to reduce the matrix residual microstresses without degrading the composite. A parametric study was conducted (ref. 2) to evaluate compliant layer properties to determine their influence on composite and constituent response. A unidirectional SiC/Ti15 metal matrix composite with fiber volume ratio varying from 0.2 to 0.4 was evaluated using two simulation methods. The first method is a three-dimensional linear finite element analysis of a nine fiber unidirectional composite system. The second method uses a micromechanics based non-linear computer code 'METCAN' that stands for METal Matrix Composites ANalyzer, which is under continuous development in-house at NASA Lewis Research Center. METCAN treats material non-linearity at the constituent level, where the behavior of the material is modeled using a multi-factor interaction equation (MFIE) to account for the time-temperature-stress dependence of a constituent's properties. More detailed information on the METCAN computer code can be found in references 3-5. In these procedures, a weak interphase is simulated by a low modulus compliant layer.

Based on the studies on compliant layers, it was observed that even a low-modulus compliant layer (about 10 percent of the matrix) is sufficient to transfer stresses between fiber and the matrix as shown in figure 1. In other words, the stresses redistribute within a short distance in metal matrix composites, except for the case when there is complete debonding. However, in general, compliant layers were found to be rather ineffective in reducing the longitudinal matrix microstresses and did not significantly increase the thermal cycles to failure of the composite system.

Effect of Partial Bonding on Composite Properties

The METCAN computer code and the three-dimensional finite element analysis were combined to evaluate the effects of partial bonding and fiber fracture on the global behavior of high temperature metal matrix composites (ref. 6). Composite ply properties were computed for various degrees of fiber-matrix debonding to evaluate the sensitivities of these properties in the presence of fiber-matrix debonding and fiber fracture in a P-100 Graphite/Copper metal matrix composite at 0.466 fiber volume ratio. It was observed that for unidirectional metal matrix composites, in general, single fiber fracture and debonding have little effect on most of the composite properties. The longitudinal thermal expansion coefficient, $\alpha_{\ell_{11}}$ and the longitudinal modulus, $E_{\ell_{11}}$ are most sensitive properties to fiber-matrix debonding. The sensitivity of $\alpha_{\ell_{11}}$ to fiber debonding, as shown in figure 2, makes it a good indicator of the level of debonding in a composite. If the value of $\alpha_{\ell_{11}}$ is above the predicted value, then the debonding of fractured fibers is suspected. The rate of change or degradation in material properties due to fiber fracture and debonding is the same at high temperatures as it is at room temperature.

FINITE ELEMENT MODEL AND MICROFRACTURE EVALUATION PROCEDURE

The finite element model used in the computational simulation procedure to evaluate composite microfracture, consists of a group of nine fibers in a three-by-three unit cell array ("nine cell model"). The unidirectional composite system consists of 35 percent fiber volume ratio (fvr) SiC/Ti15 metal matrix composite (silicon carbide fibers in titanium alloy matrix). There are 16 elements ("bays") along the length of the fiber. Each unit cell as shown in figure 3, consists of 40 hexahedron (six-sided) and 8 pentahedron (five-sided) solid elements for a total of 6912 elements and 6953 nodes in the model. The cross-plied composite has three plies with 0/90/0 lay-up, as shown in figure 4, is 30 percent fiber volume ratio SiC/Ti15 metal matrix composite. There are 6 elements ("bays") along the length of the fiber. Each unit cell is again divided into 40 hexahedron (six-sided) and 8 pentahedron (five-sided) solid elements for a total of

2592 elements and 2863 nodes. The properties of the constituents at the reference (room) temperature are shown in table I. The interphase properties are assumed to be the same as those of matrix. However, the capability exists in the finite element mesh to assign different properties for the interphase material.

To simulate fracture, duplicate nodal or grid points are placed on either side of an assumed defect. These nodal points have the same geometrical location but no connectivity exists between them, thus, in effect producing a defect of zero width. The load and boundary conditions are applied to the model through uniform boundary displacements. In a typical set of simulations, fracture is initiated in the fiber at the middle of the center cell fiber and is allowed to propagate either through the matrix or along the fiber-matrix interface. Fracture is introduced around the fiber, such that the whole fiber circumference is debonded. Similarly, the crack could be initiated in the matrix or the fiber-matrix interface. Resulting nodal forces corresponding to the applied boundary displacements are computed by finite element analysis. Comparison of these nodal forces is made for the reduction in global stiffness as the defect is propagated (perturbed), and the corresponding strain energy release rates are computed, as described below. In the case of thermal loads, symmetry boundary conditions are applied in the middle planes, so that the composite is free to move on either side. As before, strain energy release rates are computed to quantify different fracture modes and establish their hierarchy.

Strain energy release rate (SERR) is an indicator of the fracture toughness of a material. It gives a measure of the amount of energy required to propagate a defect in a material. Hence, one can make a direct comparison of damage tolerances between different microfracture configurations (modes/paths), materials and geometries. One of the methods used to calculate strain energy release rate is the crack closure method. In this method, nodal displacements and corresponding nodal forces at the crack tip location are used to determine the amount of work required to close the crack, which has been extended by an incremental amount during the propagation. This approach is a local or microfracture approach. An alternate approach is a global approach and has been used to calculate SERR herein. In this approach, applied nodal displacements and corresponding

nodal forces are used to calculate the work done to propagate the crack. Strain energy release rate, G, is then, calculated as :

$$G = \frac{dW}{dA} = \frac{1}{2} \cdot \frac{(F_2 - F_1).u}{\Delta A} \qquad (1)$$

dW : change in work done

ΔA : area of new surfaces generated

u : applied displacement at the loaded end of the model

F_1, F_2 : forces at the end nodes before and after ΔA, respectively

The above equation is simply the incremental change in work divided by the incremental change in new surface area that opens up along the path from one fracture mode to another. The applied displacement between two fracture modes is kept the same, while nodal forces required to maintain that displacement change because of the reduction in global stiffness as fracture propagates.

In the case of thermal loads, SERR is calculated by comparing the internal strain energies before and after incremental propagation. Strain energy release rate, G, is then calculated as :

$$G = \frac{dW}{dA} = \frac{1}{2} \cdot \frac{(S.E.)_2 - (S.E.)_1}{\Delta A} \qquad (2)$$

dW : incremental work done

ΔA : area of new surfaces generated

$(S.E.)_1$, $(S.E.)_2$: internal strain energy prior to and after the fracture area ΔA, respectively

The SERR was computed by using both the crack closure method and the total strain energy in the case of thermal loads. Both methods give the same results, although using the total strain energy formulation is computationally more effective and elegant. The crack closure method is used to identify the contribution of each mode of failure. In the present research, the total strain energy formulation for computing SERR is used. The advantage of using a global (total) SERR formulation is that it bypasses

local stress details, like stress gradients, that may cause convergence inconsistencies.

RESULTS/DISCUSSION

The cases studied and the results obtained therefrom are described below. Typical results are presented here, while additional discussion and results are presented in references 7-10.

MICROFRACTURE IN UNIDIRECTIONAL COMPOSITE

Longitudinal Load : Stresses are redistributed in the surrounding matrix and fibers due to the initiation and propagation of fracture. For example, when the center cell fiber is fractured in the middle plane (X/L = 0.5, figure 3), the longitudinal stress in the surrounding matrix spikes to twice those in the reference (no fracture) case. However, the increase in the longitudinal stress in the neighboring fibers is only 15 percent compared to the reference case as shown in figure 5. Hence, a premature fracture (fiber stress less than 85 percent of the typical fiber fracture stress) in one fiber is unlikely to initiate fracture in neighboring fibers.

If the crack is allowed to propagate along the fiber-matrix interface following the fiber fracture, then there is about a 10 percent reduction in global longitudinal stiffness for a fully debonded center fiber as shown in figure 6. The corresponding SERR curve is shown in figure 7(a). If the fracture initiates and propagates along the fiber-matrix interface, there is no reduction in global longitudinal stiffness and hence, the SERR is zero. If the fracture initiates in the matrix and propagates into the interphase region without fiber fracture, the reduction in global stiffness is very small and thus, SERR is also very small as shown in figure 7(b). Based on SERR curves, significant observations made for the microfracture initiation and propagation under longitudinal load are as follows :

(a) Fracture initiates in the fiber :

$$\frac{\sigma_{f11}}{S_{f11T}} > 0.85 \quad \text{leads to fracture in neighboring fibers, causing a "brittle" failure}$$

$$< 0.85 \quad \text{premature fiber fracture, if}$$

$$\frac{G_I}{G_f} < 0.5 \quad (\text{or } S_{ls} < S_{f11T}) \text{ leads to interphase debonding}$$

$$> 0.5 \quad \text{leads to fracture in neighboring fibers}$$

(b) Fracture initiates in the matrix : $(\sigma_{m11} = S_{m11T})$

$$\frac{G_I}{G_m} < 0.25 \quad (\text{or } S_{ls} < S_{m11T}) \text{ will lead to interphase debonding}$$

$$> 0.25 \quad \text{fracture will propagate in the matrix up to adjacent fibers}$$

where :

σ_{f11}, σ_{m11} : longitudinal stress in fiber and matrix respectively

S_{f11T} : fiber longitudinal strength

S_{m11T} : matrix longitudinal strength

S_{ls} : interphase shear strength

G_f, G_m, G_I : critical fracture toughness of fiber, matrix and interphase, respectively

Thus, it can be concluded that if a unidirectional composite is subjected to longitudinal (along the fiber) loading, interphase debonding does not initiate by itself. It will only occur as a follow-up of fiber or matrix fracture. Although results are not shown here, even when a substantial percentage of fibers is fractured in one plane, there is a reduction in strength in that plane. The reduction in global stiffness, however, is small and perhaps difficult to detect by conventional experiments, at least for the composite system and fiber volume ratio investigated.

Transverse Loading: If the fracture initiates in the fiber or in the matrix there is no reduction in the global transverse stiffness. However, if the crack initiates in the matrix and propagates in the fiber-matrix interface and as the fiber surface starts to debond from the matrix, there is a considerable reduction in stiffness as shown in figure 8(a). There is about

a 20 percent reduction in stiffness when 40 percent of the total fiber surface area is debonded. The corresponding SERR curve is shown in figure 8(b). Once 10 percent of the fiber surface area is debonded, it takes much less energy to drive the crack further, indicating crack propagation instability and high sensitivity of debonding extension due to transverse loading.

Bending Load: Load was applied so as to bend the specimen in the XZ-plane (figure 3). For this loading case, there is no reduction in the global bending stiffness when the crack initiates in the fiber or matrix. It was also observed that if the delamination does not extend across the full width of the specimen, the so called internal (interior) delaminations, there is no reduction in the global bending stiffness. Once the delamination extends over the whole width, then there is a reduction in bending stiffness and the corresponding SERR curve is shown in figure 9. The curve shows that once the internal delamination extends across the whole width, it is the onset of instability, i.e. the delamination can extend longitudinally at the same energy level. This type of fracture mode may be classified as shearing fracture mode (II) and is driven by the presence of interlaminar shear.

MICROFRACTURE IN CROSSPLY LAMINATES

1-1 and 2-2 Direction Loading: 1-1 and 2-2 direction loading have shown essentially the same microfracture behavior. If the crack is fiber initiated in a ply which is oriented in the loading direction, its microfracture behavior is the same as that observed in the unidirectional composite discussed earlier. If a fiber is fractured, fiber-matrix interface debonding is likely to follow instantaneously. For example, if the composite is loaded in 2-2 direction, there is about a 10 percent reduction in 2-2 direction stiffness for fully debonded center fiber as shown in figure 10(a). The corresponding SERR curve is shown in figure 10(b).

However, if the fracture initiates in the matrix, it propagates through the matrix in the neighboring plies. When the fracture hits the fiber in the neighboring ply, which is oriented perpendicular to the loading direction, the crack, then, propagates along the fiber-matrix interface. There is about an 11 percent reduction for a fully debonded fiber as shown in figure 11(a), and the corresponding SERR is shown in figure 11(b).

3-3 Direction (Through-the-thickness) Loading: When the composite is loaded in the 3-3 direction, there is no reduction in global stiffness in the 3-3 direction due to a fiber fracture only. However, if the fracture initiates in the matrix and propagates in the fiber-matrix interface, there is a gradual reduction in global stiffness in the 3-3 direction. There is approximately a 50 percent reduction in global stiffness when 70 percent of the total fiber surface area is debonded as shown in figure 12(a). The corresponding SERR curve is shown in figure 12(b). Once 10 percent of the fiber surface area is debonded, then the debonding can propagate at the same energy level. However, it was noted in the unidirectional composite subjected to through-the-thickness load that once about 10 percent fiber surface area is debonded, it takes much less energy to propagate the crack further, indicating crack propagation instability and high sensitivity of debonding extension due to 3-3 loading. Thus, the 3-3 loading is much more indicative of the interfacial conditions than the fiber or matrix fracture. Although results are not presented here, it was also observed that through-the-thickness (3-3) normal loading is much more indicative of interfacial conditions than in-plane shear loading. These results suggest a flat-wise tension test would be ideally suited to experimentally identify interfacial debonding and/or internal delaminations.

Thermally-Driven Microfracture

Various thermal loading cases were evaluated for microfracture both in unidirectional and crossply composites. Only typical results are presented here, more detailed information can be found in references 8,9.

As the SiC/Ti15 composite is cooled down from processing temperature to room temperature, the longitudinal stress in the fiber is compressive, while

the matrix longitudinal stress is tensile ($\alpha_f < \alpha_m$). Hence, during the cooldown process, the fracture is likely to initiate in the matrix. In the first case, composites were uniformly heated from room temperature to a temperature of 300 C (570 F) i.e. a ΔT of 500 F. Fracture was initiated in the matrix and various microfracture configurations were evaluated. SERR's were computed for different fracture paths by using equation (2). It was observed that the SERR's were very small. Therefore, it can be concluded that microfracture propagation is quite insensitive to temperature increases up to 260 C (500 F) from room temperature.

In the next set of simulations, the crossply composite is cooled down from 815 C to -185 C, i.e. ΔT of 1000 C (1800 F). The constituent properties at higher temperatures are computed by using a "multifactor interaction equation (MFIE)" (ref. 3-5). This equation proposes modeling the material behavior using a time-temperature-stress dependence of the constituent's properties in a "material behavior space" as follows :

$$\frac{P}{P_0} = \left[\frac{T_F - T}{T_F - T_0} \right]^n \cdot \left[\frac{S_F - \sigma}{S_F - \sigma_0} \right]^m \quad \ldots\ldots \qquad (3)$$

where :

P current property value

T temperature

S strength

σ stress

subscripts o, F reference and final values, respectively

m,n exponents

The multifactor interaction equation (3) represents gradual effects during most ranges and rapidly degrading properties near the final stages as has been observed experimentally. The exponents are determined from experimental data wherever possible, otherwise default values are used which were established from studies conducted on other materials.

Herein, the constituent properties were assumed to depend only upon temperature (m = 0). The value of the exponent n has been assumed 0.5 for the matrix and 0.25 for the fiber. When computing thermal expansion coefficients at any temperature, the value of n is assumed to be -0.5 for

the matrix and -0.25 for the fiber, as thermal expansion coefficient increases with increase in temperature. The final temperature is taken as the melting point of the constituent and reference temperature is taken as the room temperature. Constituent properties at 815 C are calculated using equation (3) as shown in table II, and are assumed to remain constant for this loading case. Fracture was again initiated in the matrix, because of the stress state in the composite, and propagated through the matrix or the interphase region. Also, the fracture was initiated and propagated in the inter-ply region to delaminate the top and middle plies. When the fracture propagates in the interphase region following the matrix fracture, SERR is very small and is shown in figure 13. Hence, the crossply composite will show debonding following the matrix fracture, and thus show ductile behavior and higher apparent fracture toughness under this type of thermal loading. However, in general, microfracture propagation under thermal loads alone is not as sensitive as it is under mechanical loads.

Thermomechanical Cyclic Loading

The METCAN computer code, mentioned earlier, was used to simulate the nonlinear stress-strain curves for a HTMMC laminate subjected to thermomechanical cyclic loading. The initiation of the local fracture and its propagation within the laminate were examined, in addition to the degradation in the constituents' strength. A brief summary of this work is presented here. For more detailed information, the reader is referred to reference 10.

The HTMMC laminate used in these simulations consisted of three plies with 0/90/0 orientation, 40 percent SiC/Ti15 composite. The composite was cooled down from processing temperature (1750 F) to room temperature (70 F), followed by a combined thermomechanical cyclic loading. This cyclic loading consisted of 300 thermal cycles between 70 F and 1000 F in addition to 10,000 bending cycles (M_{xx}) between 300 and 400 lb.-in/in applied simultaneously. The number of thermal cycles to failure is assumed to be 400, while the number of mechanical load cycles to failure is assumed to be 10^6. Following the cyclic loading, the composite was loaded monotonically under tensile load or a bending load (M_{xx}) until failure. A typical load

history curve is shown in figure 14.

The results shown here correspond to the loading case where the composite is subjected to tensile load until failure, following the processing and thermomechanical loading. The composite stress-strain curve in the longitudinal direction is shown in figure 15. The longitudinal and transverse stress-strain curves for the top (0^0) ply and the constituents are shown in figures 16 and 17 respectively. It was observed that in all cases, fracture initiated in the matrix, sometimes propagated to the fiber followed by laminate fracture (perfect bond was assumed between the matrix and the fiber). This simulation was able to detect the initiation and propagation of the fracture as shown in figures 15-17. The degradation of the fiber and matrix strength at the end of processing, thermomechanical cycling and failure is shown in figures 18-19. There is a severe degradation in the strength of constituents due to thermomechanical cyclic loading. These results demonstrate the potential capabilities of the computer code METCAN in these type of simulations.

Conclusions

Computational simulation procedures were described to evaluate the composite microfracture behavior in high temperature metal matrix composites and the effects of compliant layers and partial debonding on composite properties and microfracture initiation. These procedures are based upon three-dimensional finite element analysis and composite micromechanics equations. Significant results from these simulations are collectively summarized as follows :

1). Computational simulation procedures based on three-dimensional finite element analysis, in conjunction with strain energy release rates, are effective methods to evaluate composite microfracture under

thermo-mechanical loading.

2). Microfracture propagation in metal matrix composite laminates is generally not as sensitive to thermal loads alone as it is to mechanical loads.

3). Relatively low interfacial bond (about 10 percent of the perfect bond as simulated by a reduced modulus compliant layer) is sufficient for stress transfer in metal matrix composites.

4). Interface debonding does not occur prior to fiber or matrix fracture.

5). Longitudinal thermal expansion coefficient, α_{111} is the most sensitive parameter for determining interfacial conditions in unidirectional metal matrix composites.

6). Flat-wise tension test appears to have the potential of being a sensitive test method to evaluate experimentally the damage and extent of interfacial debonding and internal delaminations.

7). Initiation and sequence of fracture modes can be identified in metal matrix composite laminates subjected to thermomechanical cyclic loading by using METCAN computer code.

8). Thermomechanical cycling severely degrades the constituents' properties.

REFERENCES

1). Saravanos, D.A.; Murthy, P.L.N.; and Morel, M.R. : Optimum Fabrication Process for Unidirectional Metal-Matrix Composites : Computational Simulation. NASA TM-102559, 1990.

2). Caruso, J.J.; Chamis, C.C.; and Brown, H. : Parametric Studies to Determine the Effect of Compliant Layers on Metal Matrix Composite Systems. NASA TM-102465, 1990.

3). Chamis, C.C.; Murthy, P.L.N.; and Hopkins, D.A. : Computational Simulation of High Temperature Metal Matrix Composites Cyclic Behavior. NASA TM-102115, 1988.

4). Murthy, P.L.N.; Hopkins, D.A.; and Chamis, C.C. : Metal Matrix Composite Micromechanics: In-Situ Behavior Influence on Composite Properties. NASA TM-102302, 1989.

5). Chamis, C.C.; et. al. : METCAN Verification Status. NASA TM-103119, 1990.

6). Caruso, J.J.; Trowbridge, D.; and Chamis, C.C. : Finite Element Applications to Explore Effects of Partial Bonding on Metal Matrix Composite Properties. NASA TM-101482, 1989.

7) Mital, S.K.; Caruso, J.J.; and Chamis, C.C. : Metal Matrix Composites Microfracture : Computational Simulation. Computers & Structures, Vol. 37, No. 2, pp. 141-150, 1990 (Also NASA TM-103153, 1990).

8). Mital, S.K.; and Chamis, C.C. : Microfracture in High Temperature Metal Matrix Crossply Laminates, NASA TM-104381, 1991.

9). Mital, S.K.; and Chamis, C.C. : Thermally-Driven Microfracture in High Temperature Metal Matrix Composites, Proceedings of Symposium on the Mechanics of Composites at Elevated and Cryogenic Temperatures, ASME Applied Mechanics Division Meeting, Columbus, Ohio, June 16-19, 1991.

10). Gotsis, P.K. : Combined Thermal and Bending Fatigue of High-Temperature Metal-Matrix Composites: Computational Simulation, NASA TM-104354, 1991

Table I. - Properties of Constituent Materials of SiC/Ti15 at Room Temp.

	SiC fiber	Ti15 matrix	Interphase
Modulus, E (Mpsi)	62.0	12.3	12.3
Poisson's ratio ν	0.3	0.32	0.32
Shear Modulus, G (Mpsi)	23.8	4.8	4.8
Coefficient of thermal expansion, α, (ppm/ F)	1.8	4.5	4.5

Table II.- Properties of Constituent Materials of SiC/Ti15 at 815 C (1500 F)

	SiC fiber	Ti15 matrix	Interphase
Modulus, E (Mpsi)	57.0	4.3	4.3
Poisson's ratio ν	0.28	0.15	0.15
Shear Modulus, G (Mpsi)	22.4	1.9	1.9
Coefficient of thermal expansion, α, (ppm/ F)	1.96	12.8	12.8

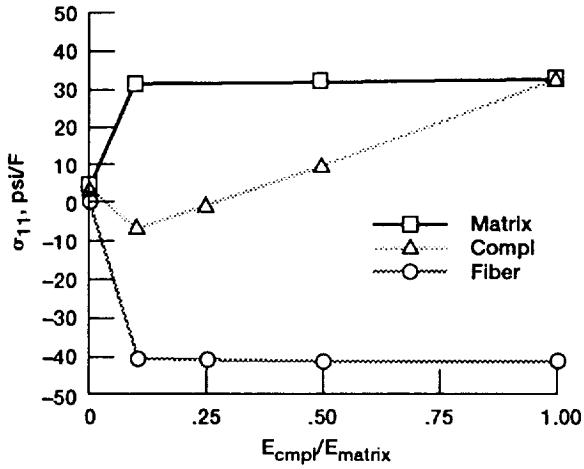

Figure 1.—Stress versus E_{cmpl}/E_m for SiCA/Ti15 L/D = 2.94, RT properties (fvr 0.46, cvr 0.01).

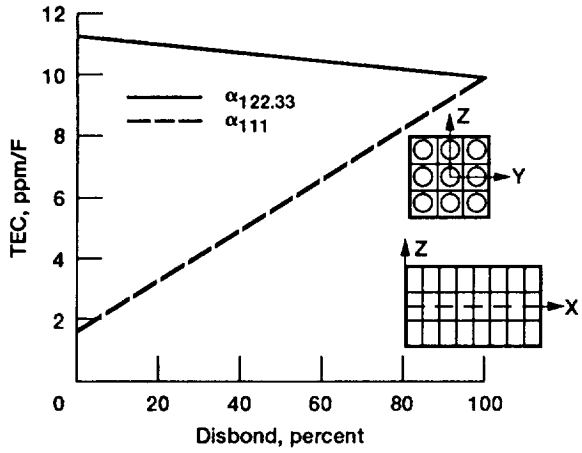

Figure 2.—Effect of fiber debonding on composite thermal expansion coefficient.

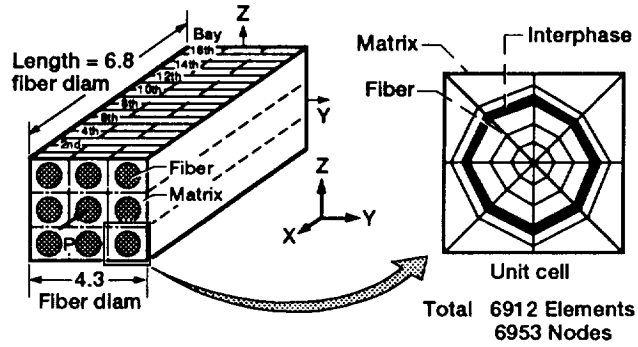

Figure 3.—Schematic of the unidirectional composite.

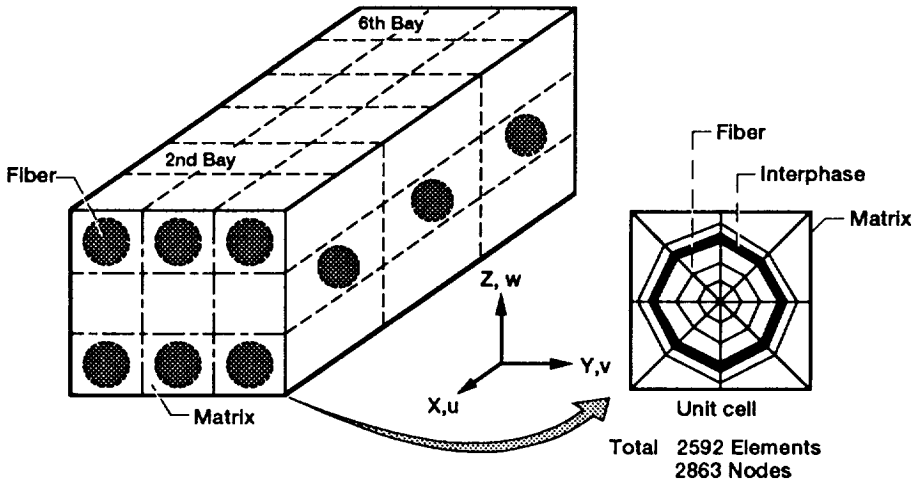

Figure 4.—Schematic of the crossply (0/90/0) composite laminate.

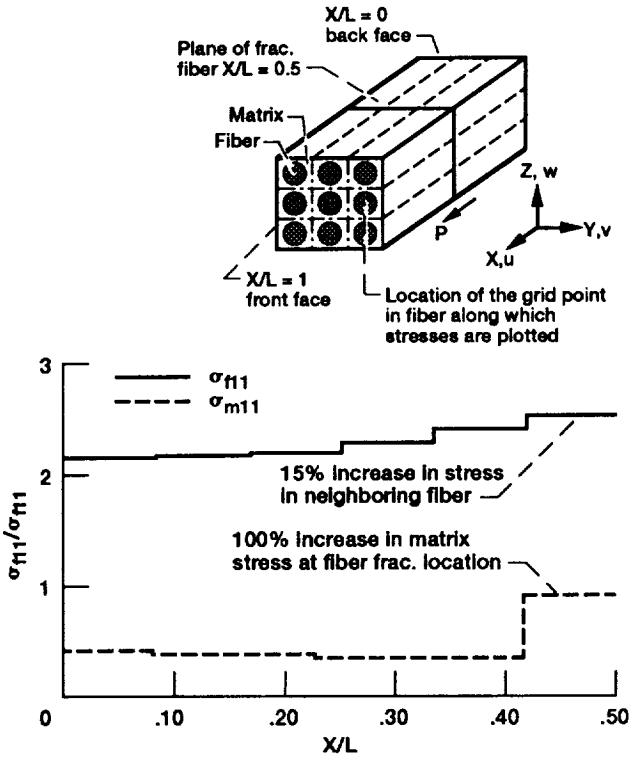

Figure 5.—Longitudinal stress variation along the length in a neighboring fiber and matrix for longitudinal loading (center cell fiber fractured at middle).

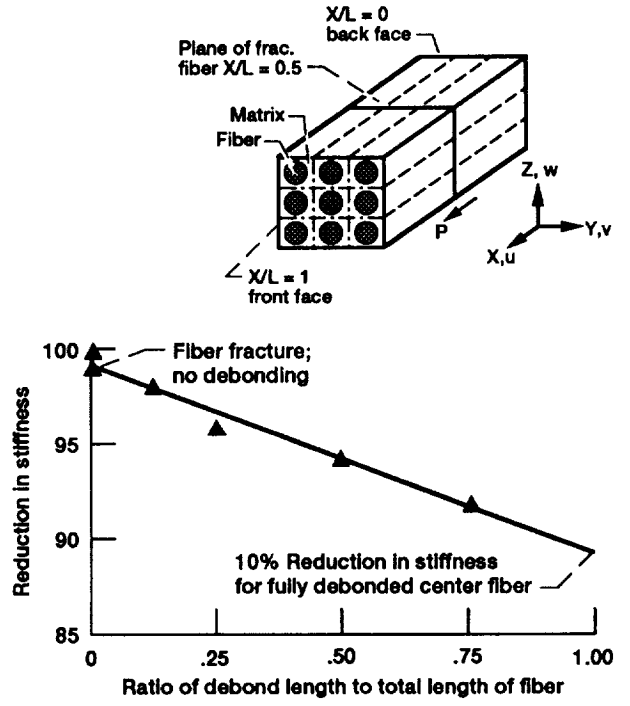

Figure 6.—Reduction in stiffness versus debond length of the center fiber (longitudinal load; unidirectional composite).

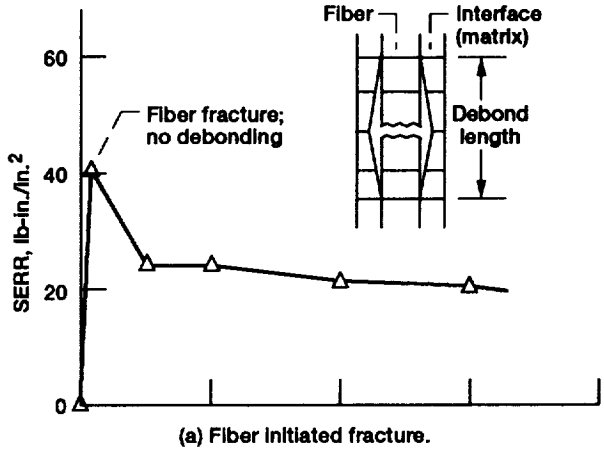

(a) Fiber initiated fracture.

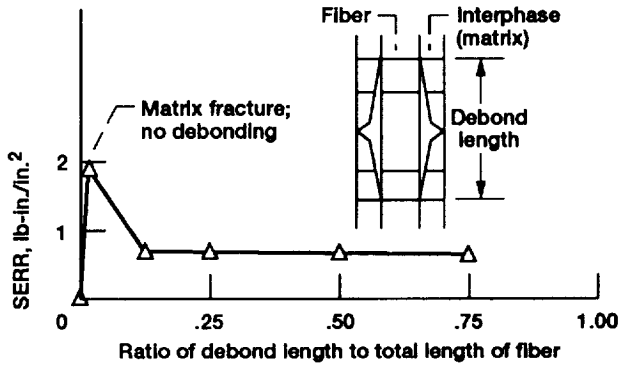

(b) Matrix initiated fracture.

Figure 7.—Strain energy release rate for center fiber debonding under longitudinal loading.

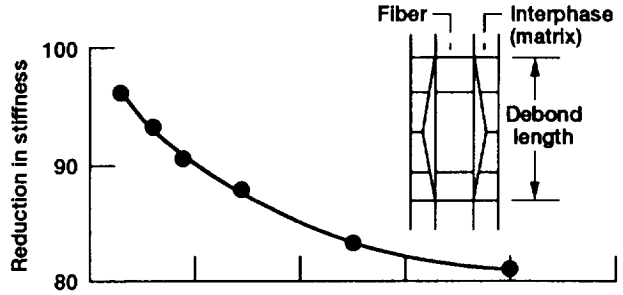

(a) Reduction in stiffness versus fiber surface area debonded under transverse loading (unidirectional composite).

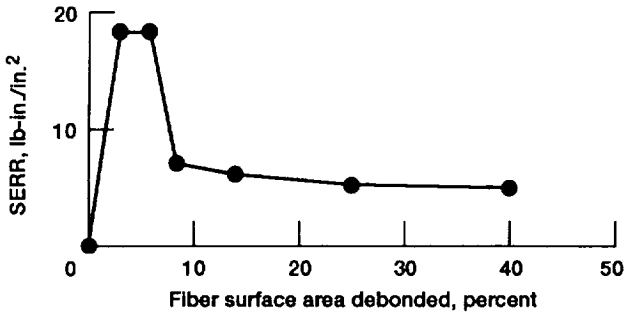

(b) Strain energy release rate versus fiber surface area debonded.

Figure 8.—Reduction in stiffness and strain energy release rate.

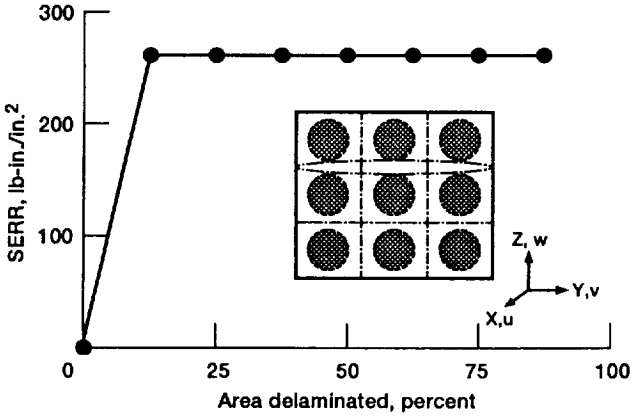

Figure 9.—Strain energy release rates versus delaminated area.

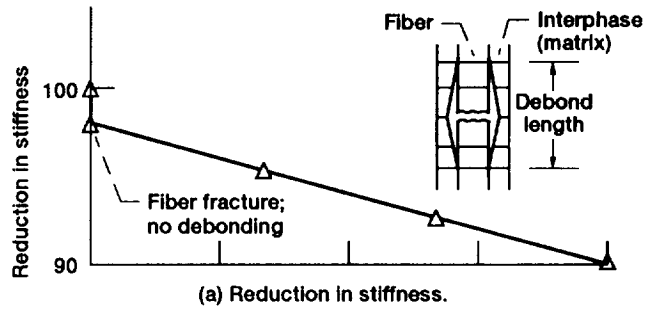

(a) Reduction in stiffness.

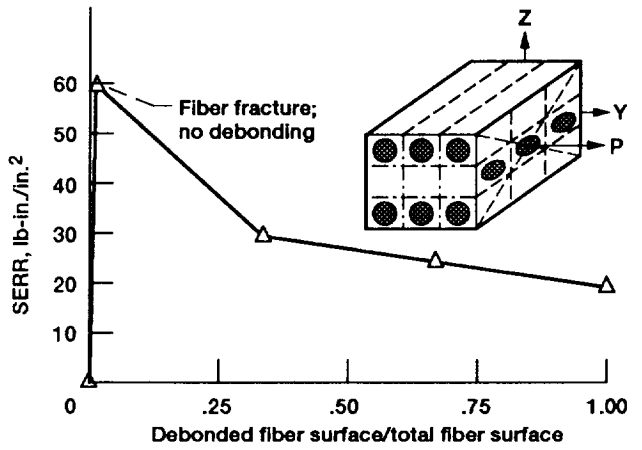

(b) Strain energy release rate.

Figure 10.—Reduction in stiffness and strain energy release rate for center cell fiber debonding under 2-2 load.

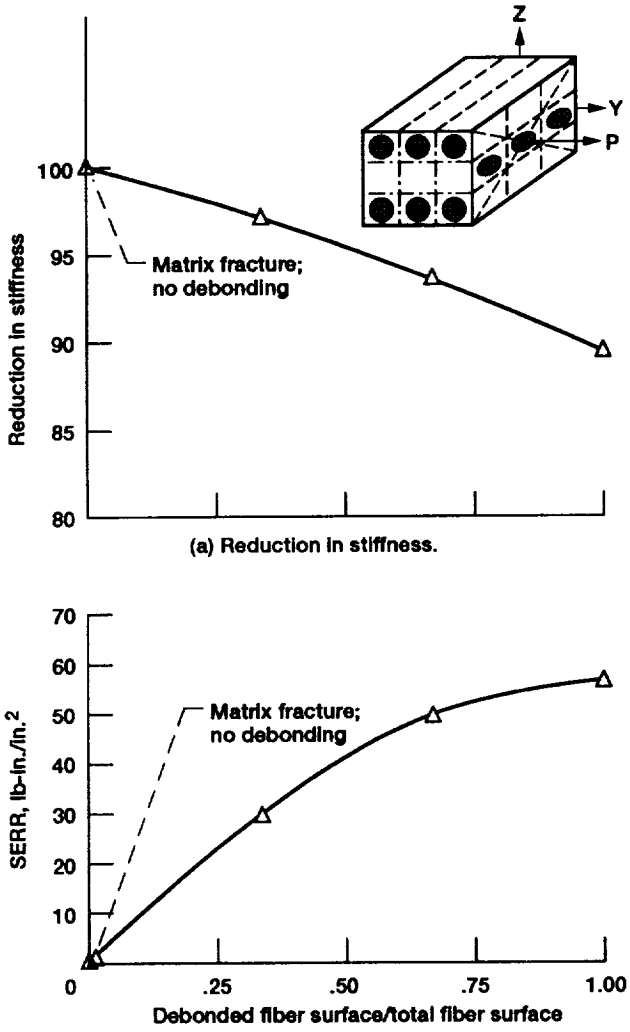

(a) Reduction in stiffness.

(b) Strain energy release rate.

Figure 11.—Reduction in stiffness and strain energy release rate for one fiber debonding under 2-2 load.

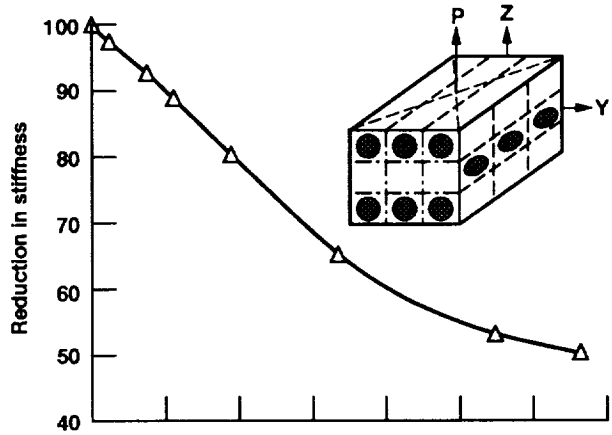

(a) Reduction in stiffness.

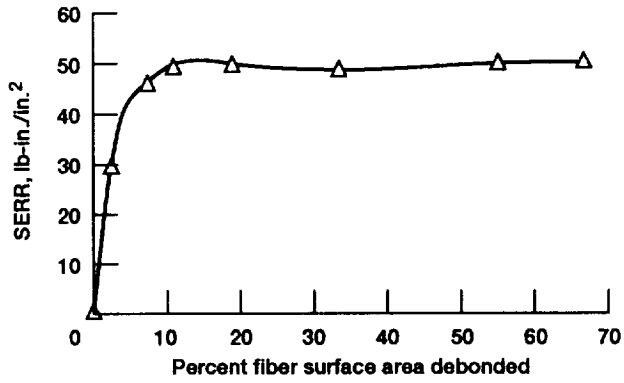

(b) Strain energy release rate.

Figure 12.—Reduction in stiffness and strain energy release rate versus percent fiber surface area debonded under 3-3 (through the thickness) load.

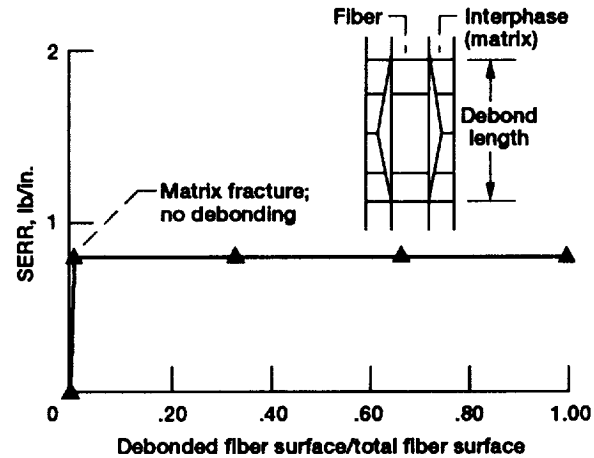

Figure 13.—Strain energy release rate for cross-ply composite; center fiber debonding under uniform cooling 815 to −185 °C.

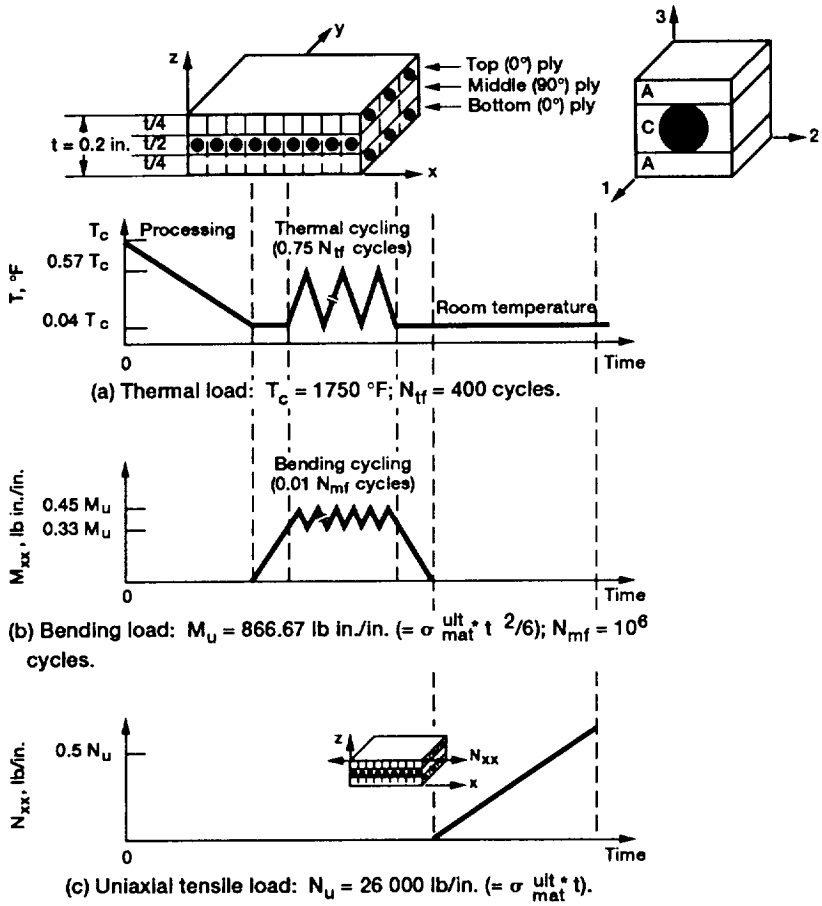

Figure 14.—Loading history.

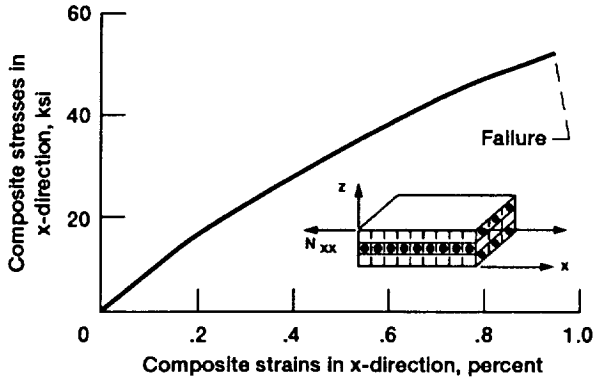

Figure 15.—Composite stress-strain curve for 1-1 direction.

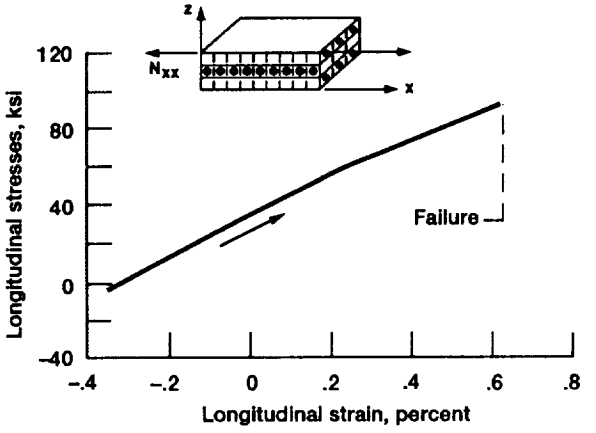

(a) Ply stresses.

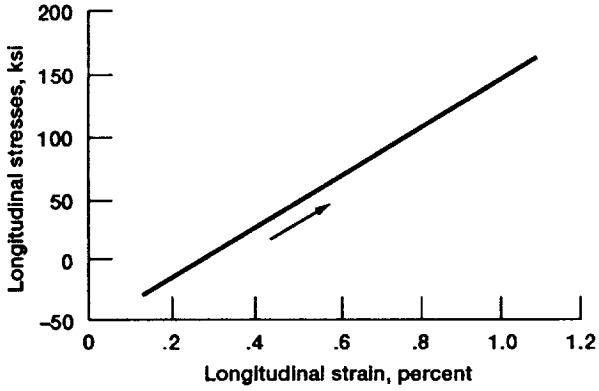

(b) Fiber microstresses.

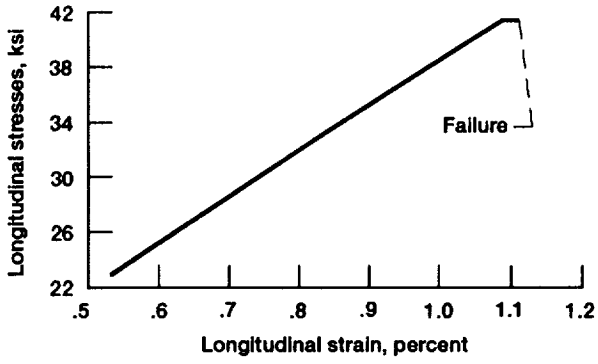

(c) Matrix microstresses at regions A and C.

Figure 16.—Longitudinal stress-strain curves for top (0 deg) ply and microstresses.

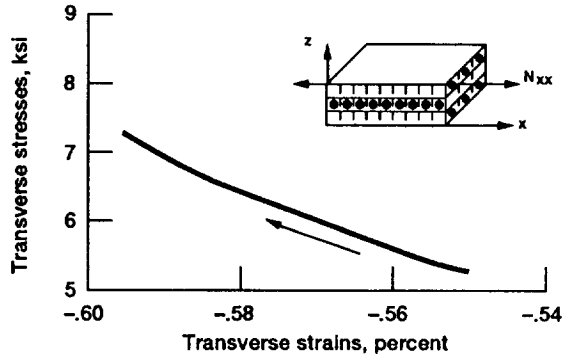

(a) Ply stresses.

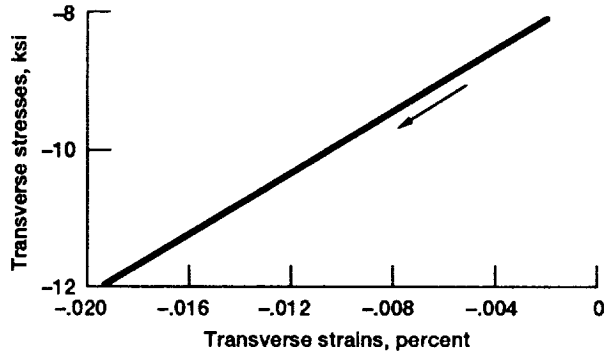

(b) Fiber microstresses.

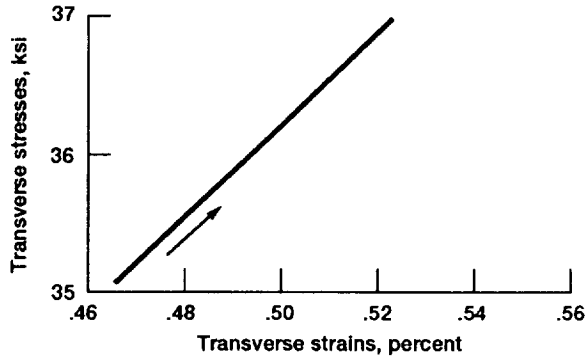

(c) Matrix microstresses in region A.

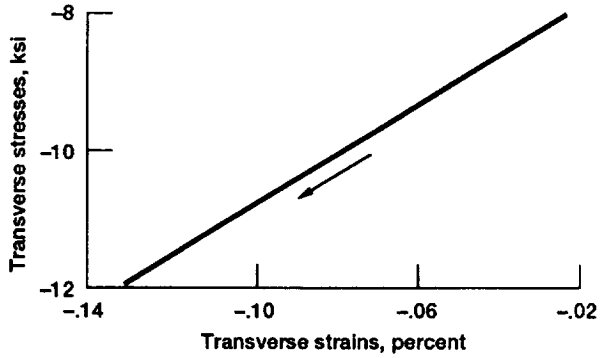

(d) Matrix microstresses in region C.

Figure 17.—Transverse stress-strain curves for top (0 deg) ply and microstresses.

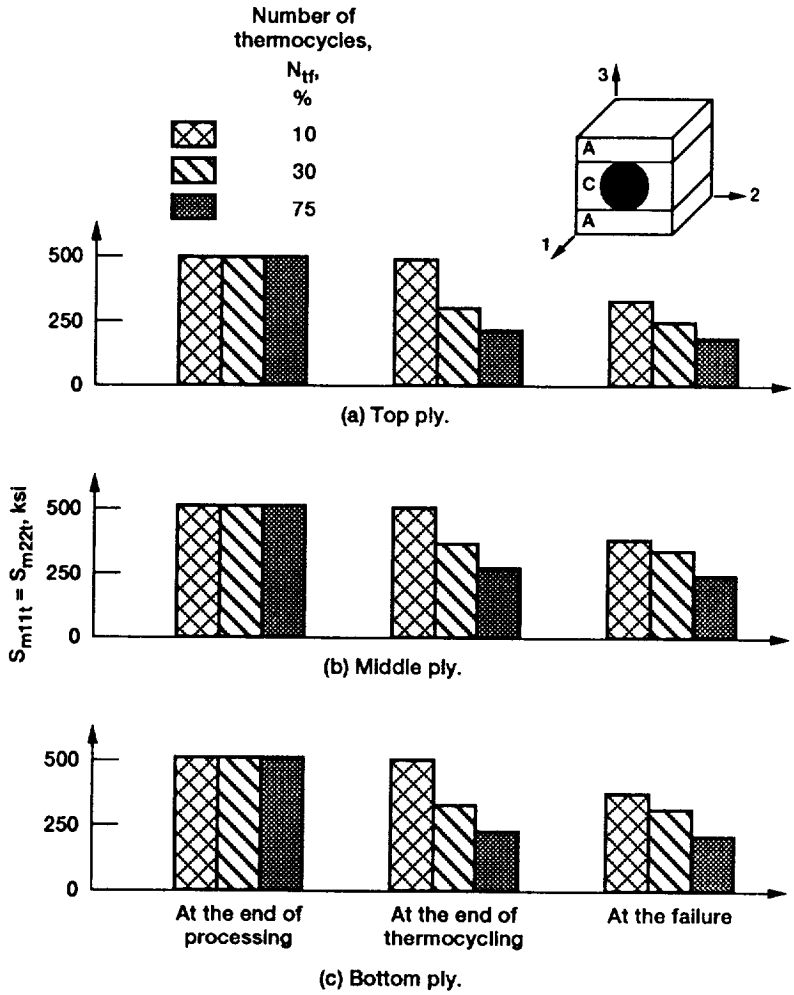

Figure 18.—Matrix tensile strength in the longitudinal and transverse directions.

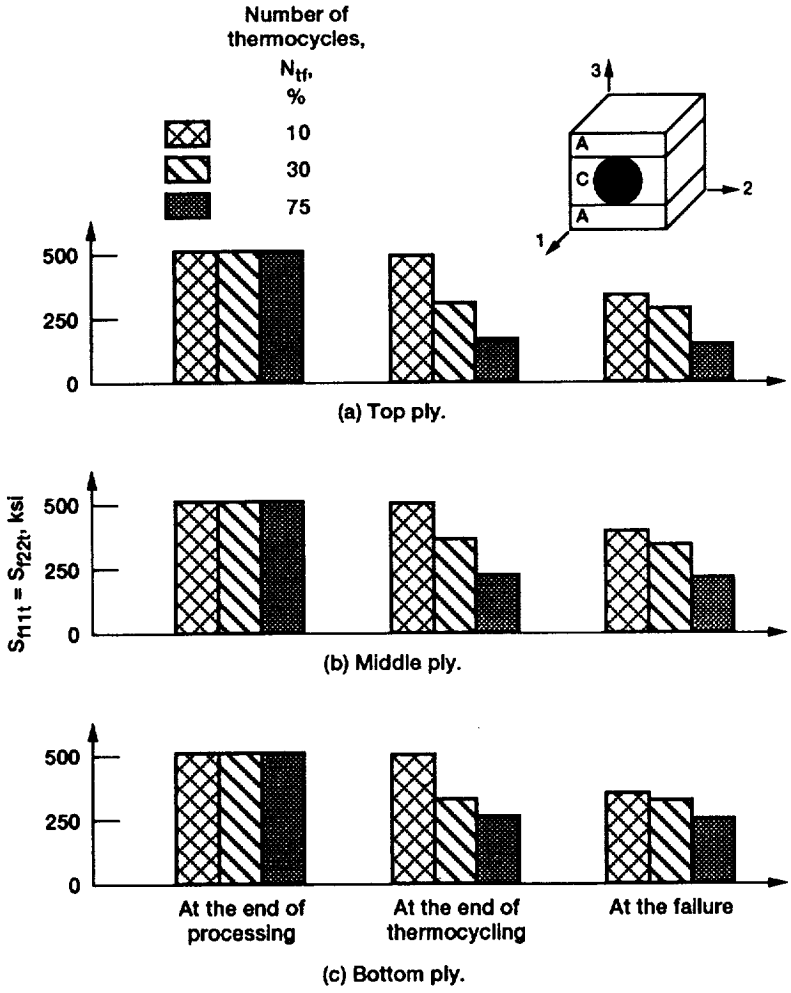

Figure 19.—Fiber tensile strength in the longitudinal and transverse directions.

REPORT DOCUMENTATION PAGE

Form Approved
OMB No. 0704-0188

1. AGENCY USE ONLY (*Leave blank*)	2. REPORT DATE	3. REPORT TYPE AND DATES COVERED
		Technical Memorandum

4. TITLE AND SUBTITLE

Microfracture in High Temperature Metal Matrix Laminates

5. FUNDING NUMBERS

WU-505-63-5B

6. AUTHOR(S)

Subodh K. Mital, Christos C. Chamis, and Pascal K. Gotsis

7. PERFORMING ORGANIZATION NAME(S) AND ADDRESS(ES)

National Aeronautics and Space Administration
Lewis Research Center
Cleveland, Ohio 44135-3191

8. PERFORMING ORGANIZATION REPORT NUMBER

E-6491

9. SPONSORING/MONITORING AGENCY NAMES(S) AND ADDRESS(ES)

National Aeronautics and Space Administration
Washington, D.C. 20546-0001

10. SPONSORING/MONITORING AGENCY REPORT NUMBER

NASA TM-105189

11. SUPPLEMENTARY NOTES

Prepared for the 32nd Structures, Structural Dynamics, and Materials Conference cosponsored by the AIAA, ASME, ASCE, AHS, and ASC, Baltimore, Maryland, April 8-10, 1991. Subodh K. Mital, University of Toledo, Toledo, Ohio 43606 (work funded by NASA Grant NAG3-1264). Christos C. Chamis and Pascal K. Gotsis, NASA Lewis Research Center. Responsible person, S.K. Mital, (216) 433-3261.

12a. DISTRIBUTION/AVAILABILITY STATEMENT

Unclassified - Unlimited
Subject Category 24

12b. DISTRIBUTION CODE

13. ABSTRACT (*Maximum 200 words*)

Computational simulation procedures are described to evaluate the composite microfracture behavior, establish the hierarchy/sequence of fracture modes and the influence of compliant layers and partial debonding on composite properties and microfracture initiation. These procedures are based upon three-dimensional finite element analysis and composite micromechanics equations. Typical results for the effects of compliant layers and partial debonding, microfracture initiation and propagation and the thermomechanical cyclic loading on SiC/Ti15 composite system are presented and discussed. The results show that interfacial debonding follows fiber or matrix fracture, and the thermomechanical cyclic loading severely degrades the composite integrity.

14. SUBJECT TERMS

Composite materials; Metal matrix composite; Microfracture; Debonding; Interface; Interphase; Matrix fracture; Fiber fracture; Strain energy release rate

15. NUMBER OF PAGES

26

16. PRICE CODE

A03

17. SECURITY CLASSIFICATION OF REPORT	18. SECURITY CLASSIFICATION OF THIS PAGE	19. SECURITY CLASSIFICATION OF ABSTRACT	20. LIMITATION OF ABSTRACT
Unclassified	Unclassified	Unclassified	